

Nonperturbative approach to the nonlinear photon echo of V-type system

Xue Zhang and Hui Dong*

*Graduate School of China Academy of Engineering Physics,
No. 10 Xibeiwang East Road, Haidian District, Beijing, 100193, China*

The analysis of nonlinear spectroscopy, widely used to study the dynamics and structures of condensed-phase matter, typically employs a perturbative approach noticing the weak interaction between the laser and the matter of interest. However, such perturbative approach is no longer applicable once the interaction between the laser and the matter is strong. We adapt the method of quantum dynamical evolution into the calculation of signal and present the response formalism of the nonlinear spectroscopy in a nonperturbative approach. In this new approach, we demonstrate that in addition to the third-order term in the perturbative method, the higher-order terms have essential contributions to the nonlinear signal of the two-pulse and three-pulse photon echo (2PPE and 3PPE). The detailed calculations are demonstrated with the example of a three-level V-type system, which is widely used in the studies of quantum optics. We consider the effect of the environment via a pure dephasing mechanism with both the localized modes of each molecule and the shared modes between molecules.

I. INTRODUCTION

Nonlinear spectroscopy is an increasingly important tool for studying the dynamics of various condensed phase systems on the femtosecond time scale[1–3]. The conventional approach[1, 4–6] to the theory of nonlinear spectroscopy utilizes a perturbative expansion to the third-order of the interaction between the external electric field and the matter of interest. The perturbative approach has provided analytical forms via the nonlinear-response functions[1, 2]. The time-domain signals measured by heterodyne detection can be attributed to the different nonlinear response functions, providing information for the underlying dynamic processes[7–11]. It has successfully explained many spectral phenomena and significantly promoted the development of nonlinear spectroscopy, especially two-dimensional spectroscopy[12, 13]. However, the calculation of optical signal in terms of nonlinear response functions is no longer applicable once the interaction between the external electric field and the matter is stronger than the interaction between electrons and nucleus or the external trap fields. For example, the strong laser field used in the photodissociation processes[14–17] is so stronger than the trap field from the nucleus that the valence electrons are ejected. And one needs alternative theoretical strategies to treat such situation with strong interaction [18–33].

The nonlinear spectroscopic signal is typically calculated via the Maxwell equation with the induced polarization vector \mathbf{P} , which is directly obtained by calculating the expected value of the polarization operator once the evolution of the wave function or the density matrix is known. In the traditional perturbative approach[1, 4–6], the wave function and density matrix are obtained through the analytical calculation with a perturbative treatment of the field-matter interaction. To go beyond, the evolutions of the system and environment need to be calculated with a nonperturbative method[18]. Here we use a trajectory method to calculate the wave function. The evolutions of the environmental degrees of freedom are mapped as trajectories in the phase space with the

coherent-state representation[34] widely used in the quantum optics. The dephasing factor induced by the environment is acquired by summing all trajectories.

In current work, we develop the nonperturbative approach to calculate the signal of the widely used photon echo spectroscopy[9, 35–38], which is an effective method to measure the homogeneous broadening in the condensed phase. The critical element of photon echo spectroscopy is to sort the echo signal from others with the phase matching mechanism according to the perturbative approach. We first prove the phase matching retained in our nonperturbative theoretical calculation. We then analytically show that the photon echo signal have contributions from terms, which is typically sorted as the higher-order terms in the standard perturbation method. With the example of the V-type three-level system, we attain the overall polarization of the system by calculating the evolution of the wave functions. We obtained fifth- and seventh-order polarization in addition to the third-order polarization, matching that in the perturbative method. We show that neglecting the higher-order terms will retain the results in the usual perturbative approach for the weak interaction. However, these higher-order terms will affect the measured dynamics in the two-dimensional spectroscopies[12, 13] when the coupling between the system and the electric field is relatively large.

The remainder of this paper is organized as follows. We introduce the basic model Hamiltonian and general notations in Sec. II. The nonperturbative procedure for calculating nonlinear spectroscopic signals of two-pulse photon echo (2PPE) with and without the environment is presented in Sec. III. The nonperturbative process for calculating nonlinear spectroscopic signals of three-pulse photon echo (3PPE) with environment is shown in Sec. IV. The comparison between the signal calculated with perturbative and nonperturbative methods are illustrated in Sec. V. Conclusions and remarks are presented in Sec. VI.

II. APPROXIMATIONS AND ASSUMPTIONS

We start by introducing the V-type system with the three levels denoted as $|g\rangle$, $|a\rangle$ and $|b\rangle$. The Hamiltonian is $H_0 =$

* hdong@gscap.ac.cn

$\hbar\omega_g |g\rangle \langle g| + \hbar\omega_a |a\rangle \langle a| + \hbar\omega_b |b\rangle \langle b|$, with $\omega_b \approx \omega_a > \omega_g$. To simplify the formula, we set the ground state energy as zero, i.e., $\omega_g = 0$. The energy level diagram is shown in Fig. 1(a). The system is coupled to the laser field with the interaction as

$$H_I = - [\hbar\Omega_a e^{-i\nu_a t + i\mathbf{k}\cdot\mathbf{r}} |a\rangle \langle g| + \text{h.c.}] - [\hbar\Omega_b e^{-i\nu_b t + i\mathbf{k}\cdot\mathbf{r}} |b\rangle \langle g| + \text{h.c.}], \quad (1)$$

where ν_a and ν_b are the frequencies of laser field with the wavevector \mathbf{k} . Here, we assume the laser field is broad enough to cover the transition from ground state to two excited states $|a\rangle$ and $|b\rangle$, and consider the resonance case: $\nu_a = \omega_a$ and $\nu_b = \omega_b$.

Before derivation, we list all the approximations to be used in this work as follows,

1. **Rotating-wave approximation.** It's already reflected in the Hamiltonian. Using the rotating-wave approximation, we ignore the high-frequency terms such as those with phase factors $e^{\pm i(\nu_a + \omega_a)t}$ and $e^{\pm i(\nu_b + \omega_b)t}$.
2. **Square pulse approximation:** We approximate the Gaussian laser pulse as a square pulse to simplify the derivation of the laser excitation process. The pulse duration is assumed to be $\delta\tau_i$ ($i = 1, 2, 3$).
3. **Initially system is on the ground state.** We also assume that the system is initially on its ground state $|\psi(0)\rangle = |g\rangle$. The light-inducing transition is around visible wavelength in the biological system with the typical energy gap of 1.55eV (corresponding to 800nm light) between the molecular ground and excited states. At room temperature, $k_B T \sim 0.026\text{eV}$ is so smaller than the energy gap that the molecules has no essential population on the excited state.
4. **Initially environment on the thermal state.** In the later discussion with system-environment interaction, we assume environmental degrees of freedom are initially on the thermal equilibrium state, $\rho_{\text{env}}(0) = \exp[-\beta H_{\text{env}}]/Z$, with $Z = \text{Tr}[\exp(-\beta H_{\text{env}})]$. Here, the detail form of Hamiltonian H_{env} for the environment will be shown in the later discussion.

The pulse sequences for the 2PPE and 3PPE experiments are illustrated in Fig. 1(b) and (c). For simplification, we use the notation $\theta_i = \Omega_i \delta\tau_i$, where $\delta\tau_i$ is the duration of the i -th pulse ($i = 1, 2$, and 3). The evolution operators for system under the laser pulses are denoted as $U_i^L(\delta\tau_i)$, while the free evolution operators are denoted as $U^0(x)$, with $x = \tau, T$, and t . The exact expressions for the the evolution operator under laser pulse are given in Appendix A.

III. TWO-PULSE PHOTON ECHO OF V-TYPE ATOMS

The photon echo experiments, including 2PPE and 3PPE, have the distinct advantage of separating homogeneous broadening from inhomogeneous broadening. To show how the nonperturbative approach works, we first investigate the

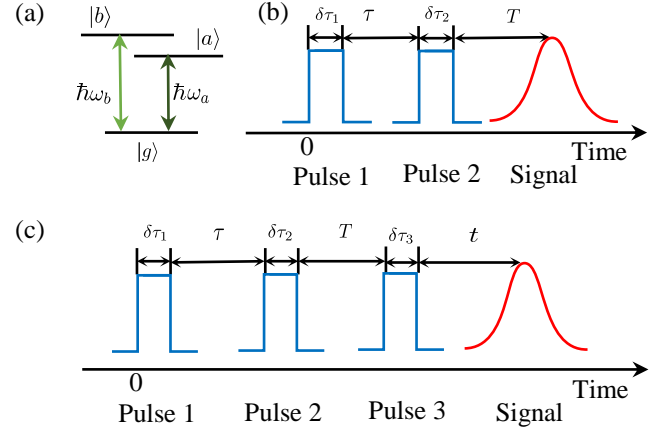


Figure 1. The energy level diagram (a) and the pulse sequence for (a) 2PPE and (b) 3PPE experiments. The squares denote the incident pump pulses under the square pulse approximation, while the dashed red lines denote the signal.

2PPE, a particular case of the 3PPE, for a V-type system without any vibrational or environmental degrees of freedom.

Assuming that the laser pulses propagate with the wave vectors \mathbf{k}_1 and \mathbf{k}_2 respectively, the signal is directly observed along the $-\mathbf{k}_1 + 2\mathbf{k}_2$ direction in the 2PPE experiment according to the nonperturbative approach. This phase matching direction will be shown to retain in the nonperturbative method in the following discussion.

The state of the system after the two pulses with a delay τ and the signal detection time T can be written as

$$|\psi_2(T, \tau)\rangle = U_0(T) U_2^L(\delta\tau_2) U_0(\tau) U_1^L(\delta\tau_1) |g\rangle. \quad (2)$$

The exact expression is shown with Eq. (B1) in Appendix B. The echo emission is obtained as the expect value of the transition dipole operator,

$$P(T, \tau) \propto \langle \psi_2(T, \tau) | \vec{\mu} | \psi_2(T, \tau) \rangle. \quad (3)$$

The transition dipole has the form with the assumption of $\mu_{ag} = \mu_{bg} = \mu$,

$$\vec{\mu} = \mu |a\rangle \langle g| + \mu |b\rangle \langle g| + \text{h.c.} \quad (4)$$

We further simplify the notation by defining $s_i = \sin\theta_i$, $c_i = \cos\theta_i$, $\eta_a = \Omega_a/\Omega$, and $\eta_b = \Omega_b/\Omega$. In any evolution operator, the wave vector \mathbf{k} is always presented in the form of a phase factor $e^{\pm i\mathbf{k}\cdot\mathbf{r}}$ as shown in Eq. (A3) of Appendix. Once the interaction between the laser pulse and the matter induces one transition, a phase factor $e^{\pm i\mathbf{k}\cdot\mathbf{r}}$, similar to that of the perturbative approach, is added. Therefore, the phase matching mechanism remains in the nonperturbative approach.

With the phase matching condition, we select the echo terms with the phase factor $\exp[i(2\mathbf{k}_2 - \mathbf{k}_1) \cdot \mathbf{r}]$,

$$-i\mu s_1 c_1 s_2^2 e^{i(2\mathbf{k}_2 - \mathbf{k}_1) \cdot \mathbf{r}} \left[\eta_a^3 e^{-i\omega_a(T-\tau)} + \eta_b^3 e^{-i\omega_b(T-\tau)} + \eta_a^2 \eta_b e^{-i\omega_b T + i\omega_a \tau} + \eta_a \eta_b^2 e^{-i\omega_a T + i\omega_b \tau} \right]. \quad (5)$$

The terms on the first line correspond to the photon echo, and the terms on the second line do not have the rephrasing ability if ω_a and ω_b are not linearly dependent. We remark here that the atoms or molecules are assumed to be spatially fixed with \mathbf{r} independent of time. Indeed, the thermal motion of atoms and molecules could induce a blur on the directional emission, yet it is not essential to break the phase matching mechanism[39].

This result is same with that obtained by the perturbative method, except for the coefficient $s_1 c_1 s_2^2$ indicating the order of terms. Therefore, we do not need to worry about the influence of higher-order terms in the 2PPE experiment. And the perturbative method is enough to analyze the properties of the system. The corresponding double-side Feynman diagrams is illustrated in Fig. 2.

We will further consider the case with dephasing coupling to the environmental degrees of freedom as

$$H = H_g |g\rangle \langle g| + H_a |a\rangle \langle a| + H_b |b\rangle \langle b|, \quad (6)$$

where

$$H_g = \sum \hbar \omega_\xi a_\xi^\dagger a_\xi + \sum \hbar \nu_\zeta b_\zeta^\dagger b_\zeta + \sum \hbar \mu_\zeta c_\zeta^\dagger c_\zeta, \quad (7)$$

$$H_a = \sum \hbar \omega_\xi [a_\xi^\dagger a_\xi + w_\xi (a_\xi^\dagger + a_\xi)] + \sum \hbar \nu_\zeta b_\zeta^\dagger b_\zeta + \sum \hbar \mu_\zeta [c_\zeta^\dagger c_\zeta + u_{a\zeta} (c_\zeta^\dagger + c_\zeta)], \quad (8)$$

$$H_b = \sum \hbar \omega_\xi a_\xi^\dagger a_\xi + \sum \hbar \nu_\zeta [b_\zeta^\dagger b_\zeta + v_\zeta (b_\zeta^\dagger + b_\zeta)] + \sum \hbar \mu_\zeta [c_\zeta^\dagger c_\zeta + u_{b\zeta} (c_\zeta^\dagger + c_\zeta)]. \quad (9)$$

Here, we assume the energy levels $|a\rangle$ and $|b\rangle$ have their own local environmental modes a_ξ and b_ζ . And the two levels also share common modes c_ζ , which could be the intermolecular vibrations. Typically, we only consider the local environmental modes in the discussion of energy transfer between molecules in the condensed phase. However, such a shared mode may exist in the strongly coupled system[40–42]. The environmental Hamiltonian H_{env} is explicitly written as $H_{\text{env}} = H_g = \sum \hbar \omega_\xi a_\xi^\dagger a_\xi + \sum \hbar \nu_\zeta b_\zeta^\dagger b_\zeta + \sum \hbar \mu_\zeta c_\zeta^\dagger c_\zeta$.

As stated in Sec. II, we assume these environmental modes are initially on the thermal equilibrium states, $\rho_{\text{env}}(0) =$

$\exp[-\beta H_{\text{env}}]/Z$. Instead of Fock space, we will use the coherent state representation to simplify the derivations[34]. The density matrix of the environment is written as

$$\rho_{\text{env}} = \bigotimes_{\xi, \zeta} \int d^2 \alpha_\xi d^2 \beta_\zeta d^2 \chi_\zeta p(\alpha_\xi, \beta_\zeta, \chi_\zeta) |\alpha_\xi \beta_\zeta \chi_\zeta\rangle \langle \alpha_\xi \beta_\zeta \chi_\zeta|, \quad (10)$$

where $|\alpha_\xi\rangle$, $|\beta_\zeta\rangle$, and $|\chi_\zeta\rangle$ are the coherent state of the harmonic oscillator modes a_ξ , b_ζ , and c_ζ , respectively. The dis-

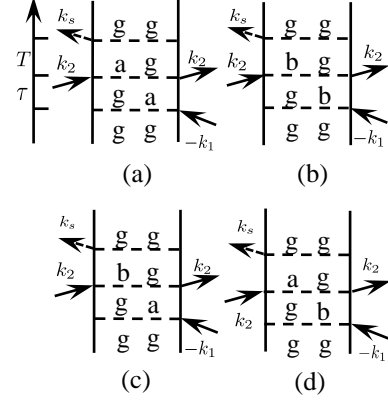


Figure 2. Double-side Feynman diagrams of 2PPE. The diagram (a), (b), (c) and (d) corresponding to the first, second, third and last term in Eq. (5). The solid and dashed arrows in the four diagrams represent the incident probe pulses and the signals, respectively.

tribution is

$$p(\alpha_\xi, \beta_\zeta, \chi_\zeta) = \prod_{\xi, \zeta} \frac{\exp \left[-\frac{|\alpha_\xi|^2}{n(\omega_\xi)} - \frac{|\beta_\zeta|^2}{n(\nu_\zeta)} - \frac{|\chi_\zeta|^2}{n(\mu_\zeta)} \right]}{\pi^3 n(\omega_\xi) n(\nu_\zeta) n(\mu_\zeta)}, \quad (11)$$

where $n(\omega)$ is mean occupation number for the state with frequency ω , i.e., $n(\omega_\xi) = \text{Tr}[a_\xi^\dagger a_\xi \rho_{\text{env}}]$, $n(\nu_\zeta) = \text{Tr}[b_\zeta^\dagger b_\zeta \rho_{\text{env}}]$ and $n(\mu_\zeta) = \text{Tr}[c_\zeta^\dagger c_\zeta \rho_{\text{env}}]$. We next consider the evolution of one arbitrary state $|g\rangle \otimes |\alpha\beta\chi\rangle$, with corresponding subscripts ignored to simplify the notation. The state of the system plus the environment after two pulses is shown with Eq.(B2) in Appendix B. The changes caused by the environment are reflected in the processes of free evolution.

Keeping the terms with factors $\exp[i(2\mathbf{k}_2 - \mathbf{k}_1) \cdot \mathbf{r}]$, we have the following contributions to the 2PPE,

$$-i\mu s_1 c_1 s_2^2 e^{i(2\mathbf{k}_2 - \mathbf{k}_1) \cdot \mathbf{r}} \times \left[\eta_a^3 e^{-i\omega_a(T-\tau)} \langle \alpha\beta\chi | e^{iH_a \tau} e^{iH_g T} e^{-iH_a T} e^{-iH_g \tau} | \alpha\beta\chi \rangle + \eta_b^3 e^{-i\omega_b(T-\tau)} \langle \alpha\beta\chi | e^{iH_b \tau} e^{iH_g T} e^{-iH_b T} e^{-iH_g \tau} | g\alpha\beta\chi \rangle + \eta_a^2 \eta_b e^{-i\omega_b T + i\omega_a \tau} \langle \alpha\beta\chi | e^{iH_a \tau} e^{iH_g T} e^{-iH_b T} e^{-iH_g \tau} | \alpha\beta\chi \rangle + \eta_a \eta_b^2 e^{-i\omega_a T + i\omega_b \tau} \langle \alpha\beta\chi | e^{iH_b \tau} e^{iH_g T} e^{-iH_a T} e^{-iH_g \tau} | \alpha\beta\chi \rangle \right]. \quad (12)$$

The first two terms characterize the photon echo signal

with phase factor $e^{-i\omega_{a(b)}(T-\tau)}$. In the following deriva-

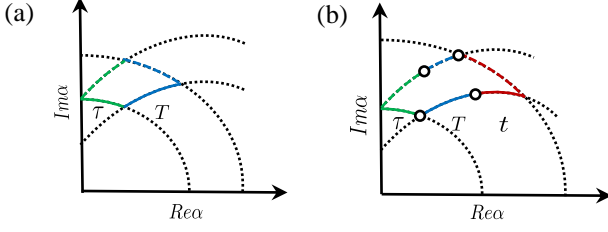


Figure 3. The evolution of the coherent state along two trajectories. (a) An example of coherent state $|\alpha\rangle$ evolution in 2PPE with evolution time τ indicated by the green line and T indicated by the blue line. (b) An example of coherent state $|\alpha\rangle$ evolution in 3PPE with evolution time τ indicated by the green line, T indicated by the blue line, and t indicated by the red line. The solid and dashed lines represent the same evolution time, but different evolution operators.

tion, we present the derivations of each term for the environmental response. Such response can be understood as the overlap between the coherent states along two trajectories governed by different evolution operators[43]. One example is illustrated in Fig. 3(a), we consider the overlap between the coherent state $|\alpha\rangle$ of the first term in Eq. (12), i.e. $\langle\alpha|e^{iH_a\tau}e^{iH_gT}e^{-iH_aT}e^{-iH_g\tau}|\alpha\rangle \rightarrow \langle\alpha|A(-\tau)B(-T)A(T)B(\tau)|\alpha\rangle$ with the definition of the evolution operators $A(\tau) \equiv e^{-i(a^\dagger a + w(a^\dagger + a))\tau}$, and $B(T) \equiv e^{-ia^\dagger a T}$. The subscription and summation symbols are ignored here. There are two evolutions of the coherent state, $A(T)B(\tau)|\alpha\rangle$ and $B(T)A(\tau)|\alpha\rangle$. The solid (dashed) green line represents the evolution of $B(\tau)$ ($A(\tau)$), and the solid (dashed) blue line represents the evolution of $A(T)$ ($B(T)$).

Here, the dephasing effect is captured by the trajectory factor,

$$\mathcal{D}_{ij}(\tau, T; \alpha\beta\chi) = \langle\alpha\beta\chi|e^{iH_i\tau}e^{iH_gT}e^{-iH_jT}e^{-iH_g\tau}|\alpha\beta\chi\rangle, \quad (13)$$

where $i, j = a, b$. The trajectory factor $\mathcal{D}_{ij}(\tau, T; \alpha\beta\chi)$ can be evaluated by the overlap between the wave functions of the two evolutions. Such dephasing is caused purely by the evolution of the environment. To measure the environmental dephasing, one must eliminate another dephasing caused by the ensemble average ω_i of the phase factors, i.e., $\exp[-i\omega_i(T - \tau)]$, ($i = a, b$) in the first two terms in Eq. (12) and $\exp[-i\omega_i T + i\omega_j \tau]$ in the last two terms in Eq. (12). In the photon echo technique, by setting $\tau = T$, the disappearance of the phase factor $\exp[-i\omega_i(T - \tau)]$ in the first two terms of Eq. (12) allows the direct observation of dephasing caused by its coupling to environment modes without any additional dephasing induced by averaging over distribution of transition frequencies (inhomogeneous broadening). The last two terms show the dephasing between two excited states $|a\rangle$, $|b\rangle$ and ground state $|g\rangle$. The inhomogeneity induced dephasing through the phase term $\exp[-i\omega_i T + i\omega_j \tau]$ ($i, j = a, b$; $i \neq j$) can not be eliminated through the photon echo if ω_i and ω_j are not linearly dependent on each other.

The total dephasing factor $D(\tau, T)$ as

$$D(\tau, T) = \prod_{\xi \leq \zeta} \int d^2\alpha_\xi d^2\beta_\zeta d^2\chi_\zeta p(\alpha_\xi, \beta_\zeta, \chi_\zeta) \mathcal{D}_{ij}(\tau, T; \alpha\beta\chi), \quad (14)$$

is easily calculated through Eq. (11) and Eq. (13). We take the first term $\mathcal{D}_{aa}(\tau, T; \alpha\beta\chi)$ as an example and derive the total dephasing factor $D_{aa}(\tau, T)$. The exact form of $\mathcal{D}_{aa}(\tau, T; \alpha\beta\chi)$ is presented with Eq. (C1) in Appendix C. A simple multivariate Gaussian integration gives the follow result,

$$D_{aa}(\tau, T) = \exp \{ -2g_a^*(\tau) - g_a^*(T) - g_a(T) + g_a^*(\tau + T) - 2\mathcal{C}_{aa}^*(\tau) - \mathcal{C}_{aa}^*(T) - \mathcal{C}_{aa}(T) + \mathcal{C}_{aa}^*(\tau + T) \}, \quad (15)$$

where

$$g_a(t, T_e) = \int d\omega \mathcal{J}_a(\omega) [(1 - \cos \omega t) \coth(\omega/2kT_e) + i(-\omega t + \sin \omega t)], \quad (16)$$

$$\mathcal{C}_{aa}(t, T_e) = \int d\mu \mathcal{J}_{aa}(\mu) [(1 - \cos \mu t) \coth(\nu/2kT_e) + i(-\nu t + \sin \nu t)]. \quad (17)$$

Here $g_a(t, T_e)$ and $\mathcal{C}_{aa}(t, T_e)$ are the lineshape functions at temperature T_e . The spectral density is defined as $\mathcal{J}_a(\omega) = \sum w_\xi^2 \delta(\omega - \omega_\xi)$ and $\mathcal{J}_{aa}(\mu) = \sum u_{a\zeta}^2 \delta(\mu - \mu_\zeta)$.

At the echo time $T = \tau$, the intensity will have the following form

$$S(\tau) = S(0) \Gamma'_{aa}(\tau), \quad (18)$$

where

$$\begin{aligned} \Gamma'_{aa}(\tau) &\equiv |D_{aa}(\tau, \tau)|^2 \\ &= \exp[-2(4P_a(\tau) + 4P_c(\tau) - P_a(2\tau) - P_c(2\tau))], \end{aligned} \quad (19)$$

with $P_a(t) = \text{Re}[g_a(t)]$, $P_c(t) = \text{Re}[\mathcal{C}_{aa}(t)]$. Until here, we have derived the well-known photon echo formalism for two-level system ($|g\rangle, |a\rangle$). And Eq. 19 clearly shows the photon echo signal intensity is determined only by system-environment coupling.

For the V-type system, we have another term

$$\begin{aligned} D_{ab}(\tau, T) &= \exp[-g_a^*(\tau) - g_b(T) - \mathcal{C}_{aa}^*(\tau) - \mathcal{C}_{bb}(T)] \\ &\times \exp[-\mathcal{C}_{ab}^*(\tau) - \mathcal{C}_{ab}^*(T) + \mathcal{C}_{ab}^*(\tau + T)], \end{aligned} \quad (20)$$

where

$$\begin{aligned} \mathcal{C}_{ab}(t, T_e) &= \int d\mu \mathcal{J}_{ab}(\mu) [(1 - \cos \mu t) \coth(\nu/2kT_e) \\ &\quad + i(-\nu t + \sin \nu t)], \end{aligned} \quad (21)$$

and the spectral density is defined as $\mathcal{J}_{ab}(\mu) = \sum u_{a\zeta} u_{b\zeta} \delta(\mu - \mu_\zeta)$. Besides the dephasing of $|g\rangle \langle a|$ during

the waiting time τ and $|b\rangle\langle g|$ during the waiting time T with the term $\exp[-g_a^*(\tau) - g_b(T)]$, we have additional dephasing due to the shared modes for the two excited states represented by the term $\exp[-\mathcal{C}_{aa}^*(\tau) - \mathcal{C}_{ab}^*(\tau) - \mathcal{C}_{ab}^*(T) - \mathcal{C}_{bb}^*(T) + \mathcal{C}_{ab}^*(\tau + T)]$.

However, the observed coherence for the delay time T and τ is always between the ground state ($|g\rangle$) and excited states ($|a\rangle$ and $|b\rangle$) illustrated by the Feynman diagrams in Fig. 2, with no access to the coherence between two excited states. To get more dynamics information about the three-level system, we will study the 3PPE and show the accessibility of observation of coherence between two excited states in the next section.

IV. THREE-PULSE PHOTON ECHO OF V-TYPE ATOMS

Sec. II demonstrates that the nonperturbative method is equivalent to the perturbative method in 2PPE spectroscopy. To show the difference between the two methods, we then study the 3PPE, a typical way to measure the homogeneous broadening.

Assuming that the three pulses propagates with the wave vectors \mathbf{k}_1 , \mathbf{k}_2 and \mathbf{k}_3 , respectively, the signal is directly ob-

served along the $-\mathbf{k}_1 + \mathbf{k}_2 + \mathbf{k}_3$ direction in the 3PPE experiment. And the phase matching direction is the same as that of the perturbative method. Here, the derivation for the system without coupling to the environment is skipped. We directly consider the V-type system with coupling to the environment. The state of the system after three pulses is

$$|\psi_3(\tau, T, t)\rangle = U_0(t) U_3^L(\delta\tau_3) U_0(T) U_2^L(\delta\tau_2) U_0(\tau) U_1^L(\delta\tau_1) |g\alpha\beta\chi\rangle, \quad (22)$$

whose exact expression is shown with Eq. (B4) in Appendix B.

Following a similar derivation procedure in 2PPE, we keep the terms with the phase factor $\exp[i(-\mathbf{k}_1 + \mathbf{k}_2 + \mathbf{k}_3) \cdot \mathbf{r}]$. It has 20 terms in total, including 8 third-order terms, 8 fifth-order terms, and 4 seventh-order terms. Here, by the number of the order, we follow the language of the perturbative methods with the assumption of weak interaction between the system and the three laser fields. Previously, the response function formalism was established based on the perturbative theory, and the higher-order (larger than third-order) terms are ignored. Compared to the traditional perturbative approach, these 20 terms corresponding to photon echo are grouped according to their order and listed as follows.

Third-order Terms: (The factor $\exp[i(-\mathbf{k}_1 + \mathbf{k}_2 + \mathbf{k}_3) \cdot \mathbf{r}]$ are ignored in the following formula. Here, $\Delta_{ab} = \omega_b - \omega_a$ is the energy spacing between the state $|a\rangle$ and $|b\rangle$.)

$$\begin{aligned} 1 & -i\mu\eta_a^3 s_1 c_1 s_2 c_2 s_3 c_3 e^{i\omega_a(\tau-t)} \langle\alpha\beta\chi| e^{iH_a\tau} e^{iH_g(T+t)} e^{-iH_a t} e^{-iH_g(T+\tau)} |\alpha\beta\chi\rangle, \\ 2 & -i\mu\eta_b^3 s_1 c_1 s_2 c_2 s_3 c_3 e^{i\omega_b(\tau-t)} \langle\alpha\beta\chi| e^{iH_b\tau} e^{iH_g(T+t)} e^{-iH_b t} e^{-iH_g(T+\tau)} |\alpha\beta\chi\rangle, \\ 3 & -i\mu\eta_a\eta_b^2 s_1 c_1 s_2 c_2 s_3 c_3 e^{i\omega_b\tau - i\omega_a t} \langle\alpha\beta\chi| e^{iH_b\tau} e^{iH_g(T+t)} e^{-iH_a t} e^{-iH_g(T+\tau)} |\alpha\beta\chi\rangle, \\ 4 & -i\mu\eta_a^2\eta_b s_1 c_1 s_2 c_2 s_3 c_3 e^{i\omega_a\tau - i\omega_b t} \langle\alpha\beta\chi| e^{iH_a\tau} e^{iH_g(T+t)} e^{-iH_b t} e^{-iH_g(T+\tau)} |\alpha\beta\chi\rangle, \\ 5 & -i\mu\eta_a^3 s_1 c_1 s_2 s_3 (\eta_b^2 + \eta_a^2 c_2)(\eta_b^2 + \eta_a^2 c_3) e^{i\omega_a(\tau-t)} \langle\alpha\beta\chi| e^{iH_a(\tau+T)} e^{iH_g t} e^{-iH_a(t+T)} e^{-iH_g\tau} |\alpha\beta\chi\rangle, \\ 6 & -i\mu\eta_b^3 s_1 c_1 s_2 s_3 (\eta_a^2 + \eta_b^2 c_2)(\eta_a^2 + \eta_b^2 c_3) e^{i\omega_b(\tau-t)} \langle\alpha\beta\chi| e^{iH_b(\tau+T)} e^{iH_g t} e^{-iH_b(t+T)} e^{-iH_g\tau} |\alpha\beta\chi\rangle, \\ 7 & -i\mu\eta_a\eta_b^2 s_1 c_1 s_2 s_3 (\eta_a^2 + \eta_b^2 c_2)(\eta_b^2 + \eta_a^2 c_3) e^{i\omega_b\tau - i\omega_a t + i\Delta_{ab}T} \langle\alpha\beta\chi| e^{iH_b(\tau+T)} e^{iH_g t} e^{-iH_a(t+T)} e^{-iH_g\tau} |\alpha\beta\chi\rangle, \\ 8 & -i\mu\eta_a^2\eta_b s_1 c_1 s_2 s_3 (\eta_b^2 + \eta_a^2 c_2)(\eta_a^2 + \eta_b^2 c_3) e^{i\omega_a\tau - i\omega_b t - i\Delta_{ab}T} \langle\alpha\beta\chi| e^{iH_a(\tau+T)} e^{iH_g t} e^{-iH_b(t+T)} e^{-iH_g\tau} |\alpha\beta\chi\rangle. \quad (23) \end{aligned}$$

Fifth-order Terms:

$$\begin{aligned} 9 & -i\mu\eta_a^3\eta_b^2 s_1 c_1 s_2 (c_2 - 1) s_3 (\eta_b^2 + \eta_a^2 c_3) e^{i\omega_b\tau - i\omega_a t} \langle\alpha\beta\chi| e^{iH_b\tau} e^{iH_a T} e^{iH_g t} e^{-iH_a(t+T)} e^{-iH_g\tau} |\alpha\beta\chi\rangle, \\ 10 & -i\mu\eta_a^2\eta_b^3 s_1 c_1 s_2 (c_2 - 1) s_3 (\eta_a^2 + \eta_b^2 c_3) e^{i\omega_a\tau - i\omega_b t} \langle\alpha\beta\chi| e^{iH_a\tau} e^{iH_b T} e^{iH_g t} e^{-iH_b(t+T)} e^{-iH_g\tau} |\alpha\beta\chi\rangle, \\ 11 & -i\mu\eta_a^4\eta_b s_1 c_1 s_2 (\eta_b^2 + \eta_a^2 c_2) s_3 (c_3 - 1) e^{i\omega_a\tau - i\omega_b t} \langle\alpha\beta\chi| e^{iH_a(\tau+T)} e^{iH_g t} e^{-iH_b t} e^{-iH_a T} e^{-iH_g\tau} |\alpha\beta\chi\rangle, \\ 12 & -i\mu\eta_a\eta_b^4 s_1 c_1 s_2 (\eta_a^2 + \eta_b^2 c_2) s_3 (c_3 - 1) e^{i\omega_b\tau - i\omega_a t} \langle\alpha\beta\chi| e^{iH_b(\tau+T)} e^{iH_g t} e^{-iH_a t} e^{-iH_b T} e^{-iH_g\tau} |\alpha\beta\chi\rangle, \\ 13 & -i\mu\eta_a^3\eta_b^2 s_1 c_1 s_2 (c_2 - 1) s_3 (\eta_b^2 + \eta_a^2 c_3) e^{i\omega_a\tau - i\omega_a t + i\Delta_{ab}T} \langle\alpha\beta\chi| e^{iH_a\tau} e^{iH_b T} e^{iH_g t} e^{-iH_a(t+T)} e^{-iH_g\tau} |\alpha\beta\chi\rangle, \\ 14 & -i\mu\eta_a^2\eta_b^3 s_1 c_1 s_2 (c_2 - 1) s_3 (\eta_a^2 + \eta_b^2 c_3) e^{i\omega_b\tau - i\omega_b t - i\Delta_{ab}T} \langle\alpha\beta\chi| e^{iH_b\tau} e^{iH_a T} e^{iH_g t} e^{-iH_b(t+T)} e^{-iH_g\tau} |\alpha\beta\chi\rangle, \\ 15 & -i\mu\eta_a^2\eta_b^3 s_1 c_1 s_2 (\eta_a^2 + \eta_b^2 c_2) s_3 (c_3 - 1) e^{i\omega_b\tau - i\omega_b t + i\Delta_{ab}T} \langle\alpha\beta\chi| e^{iH_b(\tau+T)} e^{iH_g t} e^{-iH_b t} e^{-iH_a T} e^{-iH_g\tau} |\alpha\beta\chi\rangle, \\ 16 & -i\mu\eta_a^3\eta_b^2 s_1 c_1 s_2 (\eta_b^2 + \eta_a^2 c_2) s_3 (c_3 - 1) e^{i\omega_a\tau - i\omega_a t - i\Delta_{ab}T} \langle\alpha\beta\chi| e^{iH_a(\tau+T)} e^{iH_g t} e^{-iH_a t} e^{-iH_b T} e^{-iH_g\tau} |\alpha\beta\chi\rangle. \quad (24) \end{aligned}$$

Seventh-order Terms:

$$\begin{aligned}
17 & -i\mu\eta_a^3\eta_b^4s_1c_1s_2(c_2-1)s_3(c_3-1)e^{i\omega_a(\tau-t)}\langle\alpha\beta\chi|e^{iH_a\tau}e^{iH_bT}e^{iH_gt}e^{-iH_at}e^{-iH_bT}e^{-iH_g\tau}|\alpha\beta\chi\rangle, \\
18 & -i\mu\eta_a^4\eta_b^3s_1c_1s_2(c_2-1)s_3(c_3-1)e^{i\omega_b(\tau-t)}\langle\alpha\beta\chi|e^{iH_b\tau}e^{iH_aT}e^{iH_gt}e^{-iH_bt}e^{-iH_aT}e^{-iH_g\tau}|\alpha\beta\chi\rangle, \\
19 & -i\mu\eta_a^4\eta_b^3s_1c_1s_2(c_2-1)s_3(c_3-1)e^{i\omega_a\tau-i\omega_bt+i\Delta_{ab}T}\langle\alpha\beta\chi|e^{iH_a\tau}e^{iH_bT}e^{iH_gt}e^{-iH_bt}e^{-iH_aT}e^{-iH_g\tau}|\alpha\beta\chi\rangle, \\
20 & -i\mu\eta_a^3\eta_b^4s_1c_1s_2(c_2-1)s_3(c_3-1)e^{i\omega_b\tau-i\omega_at-i\Delta_{ab}T}\langle\alpha\beta\chi|e^{iH_b\tau}e^{iH_aT}e^{iH_gt}e^{-iH_at}e^{-iH_bT}e^{-iH_g\tau}|\alpha\beta\chi\rangle. \quad (25)
\end{aligned}$$

In the perturbative approach, the terms **9-20** are not considered due to their negligible contributions to total photon echo signal intensity. In all responses of the third-order, terms **1-4** represent the ground state dynamics $|g\rangle\langle g|$ during the second delay time T , while term 5 (6) corresponds to the dynamics of the excited state $|a\rangle\langle a|$ ($|b\rangle\langle b|$). The corresponding double-side Feynman diagrams are illustrated in Fig. 4.

We next utilize two-dimensional spectroscopy, a powerful experimental technique that probes the nonlinear optical response of materials, to study the effect of higher-order terms on the signal. In essence, the traditional “1D” spectroscopy, which measures the linear response, reveals the excitations in a system, whereas the two-dimensional spectroscopy reveals the dynamics caused by these excitations[44]. Through the two-dimensional spectroscopy, we get the dynamics of the system and explain spectral phenomena.

To get the two-dimensional spectrum $S_i(\omega_\tau, T, \omega_t)$, we apply Fourier transform for the first and third delay times t and τ to get the two-dimensional spectrum, namely, $S_i(\omega_\tau, T, \omega_t) = \mathcal{F}[R_i(\tau, T, t)]$ ($i=1, 2, \dots, 20$). For example, the Fourier transform of term 1 results in a peak around $(\omega_a, -\omega_a)$, noticing the response term of the environment will not present a significant change of oscillation frequencies during the first and third waiting times t and τ . In the later discussion, we will flip the sign of the second axis to be positive as $S'_i(\omega_\tau, T, \omega_t) \equiv S_i(\omega_\tau, T, -\omega_t)$ and give the signal as $|S'_i(\omega_\tau, T, \omega_t)|^2$.

We group the 20 response terms based on their position on the two-dimensional spectrum and show them in Table I. During the waiting time T , the coherence dynamics for signal calculated by the traditional perturbative method at the off-diagonal peak (ω_a, ω_b) show a beating with the frequency as energy difference Δ_{ab} between two excited states, which is contributed by the term 8. However, due to the contribution of an additional higher-order term 19, the coherence dynamics in our nonperturbative method at the off-diagonal peak (ω_a, ω_b) exhibit different oscillations at frequencies Δ_{ab} and $2\Delta_{ab}$. We have contributions from higher-order terms to the dynamics of each peak.

In the traditional perturbative method, the design of the 3PPE allows the direct probe of the dephasing between the two electronic energy levels $|a\rangle$ and $|b\rangle$ via the off-diagonal terms. The oscillation pattern enables the separation of coherence dynamics from population dynamics and we can get more information about the molecules, which is why 3PPE is commonly used with respect to 2PPE.

The decoherence factor for 3PPE is different from that in 2PPE, especially for the processes with the coherence dynamics along delay time T . A schematic diagram of the evolution of the coherent state $|\alpha\rangle$ in term 8 is illustrated in

Position	terms	order	T dynamics
(ω_a, ω_b)	4	third-order	ground state $ g\rangle\langle g $
	8	third-order	coherence $ b\rangle\langle a $
	10	fifth-order	excited state $ b\rangle\langle b $
	11	fifth-order	excited state $ a\rangle\langle a $
	19	seventh-order	coherence $ a\rangle\langle b $
(ω_b, ω_a)	3	third-order	ground state $ g\rangle\langle g $
	7	third-order	coherence $ a\rangle\langle b $
	9	fifth-order	excited state $ a\rangle\langle a $
	12	fifth-order	excited state $ b\rangle\langle b $
	20	seventh-order	coherence $ b\rangle\langle a $
(ω_a, ω_a)	1	third-order	ground state $ g\rangle\langle g $
	5	third-order	excited state $ a\rangle\langle a $
	13	fifth-order	coherence $ a\rangle\langle b $
	16	fifth-order	coherence $ b\rangle\langle a $
	17	seventh-order	excited state $ b\rangle\langle b $
(ω_b, ω_b)	2	third-order	ground state $ g\rangle\langle g $
	6	third-order	excited state $ b\rangle\langle b $
	14	fifth-order	coherence $ b\rangle\langle a $
	15	fifth-order	coherence $ a\rangle\langle b $
	18	seventh-order	excited state $ a\rangle\langle a $

Table I. Classification of 20 terms. These 20 terms are divided into 4 categories according to their spectral positions on the two-dimensional Fourier spectrum. We also list the corresponding order and T -time dynamics of each term.

Fig. 3(b). There are two evolutions of the coherent state, $e^{-iH_b(t+T)}e^{-iH_g\tau}|\alpha\rangle$ and $e^{-iH_gt}e^{-iH_a(\tau+T)}|\alpha\rangle$. The red lines represents the evolution of t . We only consider the environmental factor in the coherence pathway of term 8. The trajectory decoherence factor for term 8 is $\mathcal{D}_8(\tau, T, t; \alpha, \beta, \chi)$, presented in Eq. (C2) in Appendix C. The integration over all the trajectories with the weight function $p(\alpha_\xi, \beta_\zeta, \chi_\zeta)$ results in the decoherence factor

$$\begin{aligned}
D_8(\tau, T, t) = \exp & [-g_a^*(T + \tau) - g_b(t + T) - \mathcal{C}_{aa}^*(T + \tau) \\
& - \mathcal{C}_{bb}(t + T) + \mathcal{C}_{ab}^*(T + t + \tau) \\
& - \mathcal{C}_{ab}^*(\tau) + \mathcal{C}_{ab}(T) - \mathcal{C}_{ab}^*(t)]. \quad (26)
\end{aligned}$$

Decoherence factors for all terms in Sec. IV are presented in Appendix D.

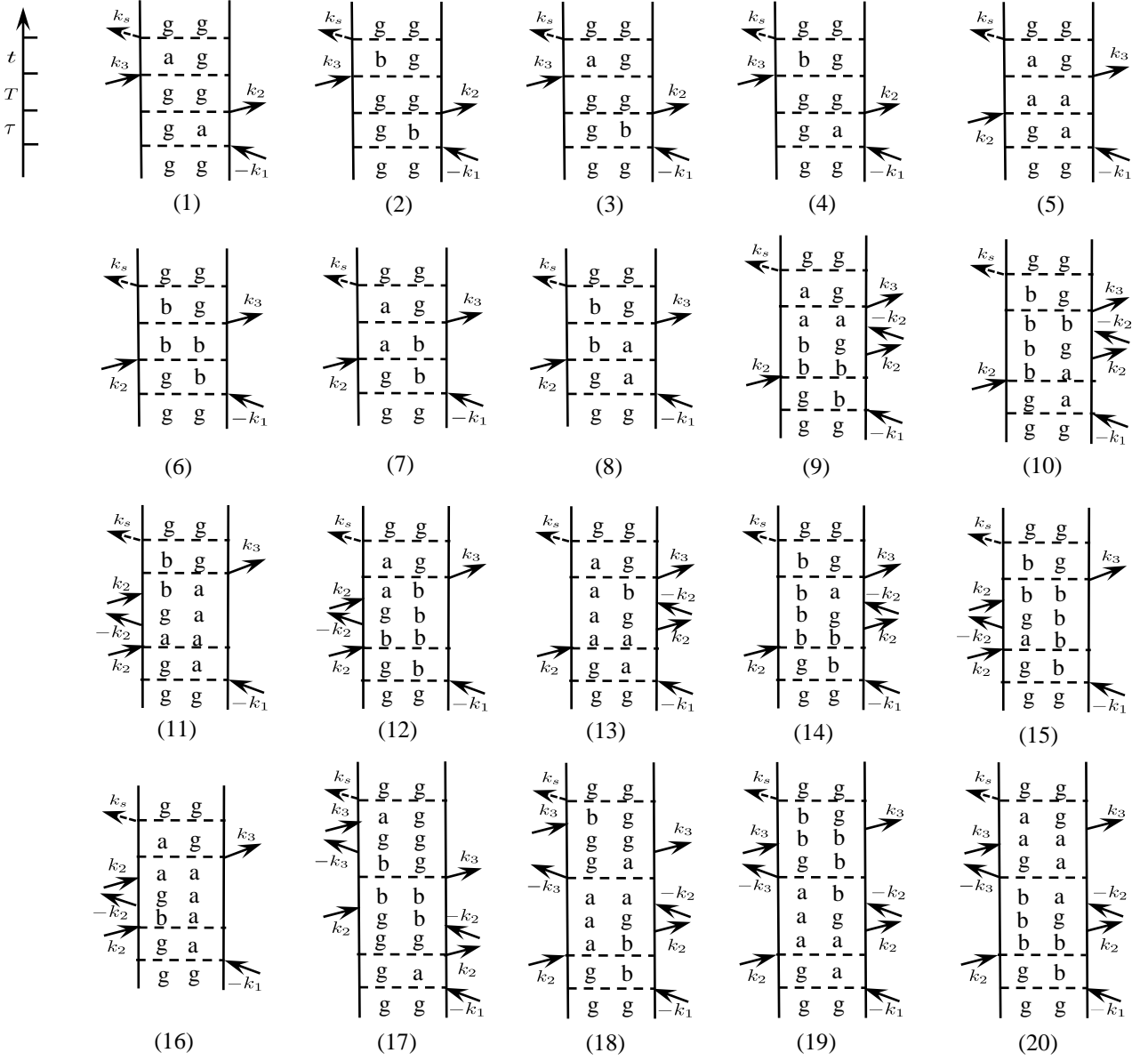


Figure 4. Double-side Feynman diagrams for 20 terms in 3PPE. (1)-(8) third-order terms in Eq. (23), (9)-(16) fifth-order terms in Eq. (24) and (17)-(20) seventh-order terms in Eq. (25). The sequence numbers (1)-(20) are consistent with that in 20 terms. The solid and dashed arrows in the three diagrams are the same as Fig. 2.

V. COMPARISONS

In the two sections above, we have derived both the 2PPE and 3PPE formalism with the nonperturbative method. To compared with the traditional perturbative approach, we focus on the 3PPE, and discuss the effect brought by the higher-order terms.

For simplicity, we use the well-known Kubo stochastic model[45], where the lineshape function is given by[46]

$$g(t) = (\Delta\tau_0)^2 [e^{-t/\tau_0} + \frac{t}{\tau_0} - 1]. \quad (27)$$

Here τ_0 is the environmental correlation time, and Δ is the fluctuation amplitude of the excited states induced by the coupling to the environment. To clarify the advantage of our non-perturbative approach, we first consider the case where levels $|a\rangle$ and $|b\rangle$ don't have shared environmental modes c_c , namely $\mathcal{C}_{aa}(t) = 0$, $\mathcal{C}_{bb}(t) = 0$ and $\mathcal{C}_{ab}(t) = 0$. And we also assume the equal coupling strength $w_\xi = v_\zeta$, which implies $g_a(t) = g_b(t) = g(t)$. The correlation time and fluctuation amplitude are chosen as $\tau_0 = 1\text{ps}$ and $\Delta = 15\text{cm}^{-1}$, respectively. The pulse durations are 35fs. The energy level gaps of the two excited states are $\omega_a = 1.25 \times 10^4\text{cm}^{-1}$ and $\omega_b = 1.31 \times 10^4\text{cm}^{-1}$, respectively.

Fig. 5 shows the 3PPE signal of the V-type system with

relatively small coupling strengths $\Omega_a = 53\text{cm}^{-1}$ and $\Omega_b = 53\text{cm}^{-1}$. The first row (a-d) show the signal calculated from the conventional perturbative approach and the second row (e-h) show the signal obtained with our nonperturbative approach. Through the vertical comparison of (a) and (e), (b) and (f), (c) and (g), (d) and (h), we find that the spectral features are roughly the same for both two methods. We also compare the dynamics along the waiting time T in Fig. 5(i). The blue and red lines are the evolution of diagonal peak (ω_a, ω_a) and off-diagonal peak (ω_a, ω_b) for the third-order terms; meanwhile, the green and cyan lines are the evolution of diagonal peak (ω_a, ω_a) and off-diagonal peak (ω_a, ω_b) for the total-order terms. The slight oscillation of the solid blue line is caused by the discrete Fourier transform. It's clear that the dynamics along the waiting time T are basically the same for both the diagonal and off-diagonal peaks. The oscillation of the green line comes from the fifth-order coherence terms 13 and 16, yet is relatively small. The red and cyan lines are almost identical, indicating the same information containing coherence terms that cause vibrations, and the coherence brought about by higher-order terms can be ignored.

Now, we turn to the case with strong couplings. In Eq. (23), Eq. (24) and Eq. (25), the coupling strengths between the laser and the matter only affect the formula coefficients s_i and c_i , which vary periodically with the coupling strength. Therefore, we only consider relatively strong coupling strengths $\Omega\delta\tau \sim \pi/4$. In Fig. 6, the coupling strengths are $\Omega_a = 106\text{cm}^{-1}$ and $\Omega_b = 106\text{cm}^{-1}$. We find that the spectral features are roughly the same in Fig. 6(a)-(h) for both two methods. However, the distinctly different evolution over waiting time T is presented in Fig. 6(i) between perturbative and nonperturbative methods. The green line has a larger additional oscillation than the blue line, and the cyan line also has different oscillation compared to the red line. To learn more about these oscillations, we perform discrete Fourier transforms of the signal in Fig. 6(i) scanned from 0 to 500 fs with 0.5fs time step for time T , the result is shown in Fig. 6(j). To compare the effects of higher-order terms on the signals of the diagonal and off-diagonal peaks, respectively, the blue solid and green dashed lines share the left y-axis, and the red solid and cyan dashed lines share the right y-axis. There are two frequencies $\omega_1 \sim \Delta_{ab}$ and $\omega_2 \sim 2\Delta_{ab}$. The two oscillation frequencies of the green line are the result of the contribution of terms 13 and 16 to the signal. The oscillation frequency ω_1 in the red line is the result of the contribution of the term 8 to the signal. Due to the contribution of the term 19 in the higher-order terms to the signal, the cyan line has an oscillation ω_2 compared to the red line. Clearly, the high-order

terms will modify the dynamics presented in the signal, and cannot be ignored in strong interaction.

To clarify the influence of the shared modes, we next consider the case where levels $|a\rangle$ and $|b\rangle$ have shared environmental modes c_ζ with the same coupling strength $u_{a\zeta} = u_{b\zeta} = u_\zeta$, namely $\mathcal{C}_{aa}(t) = \mathcal{C}_{bb}(t) = \mathcal{C}_{ab}(t)$. Here, we still use the Kubo model with the lineshape function Eq. (27). And we assume the equal coupling strength $w_\xi = v_\zeta = u_\zeta$, which implies the parameters in lineshape function are identical for the three environmental modes.

We consider the same coupling strengths with Fig. 6, and the results are presented in Fig. 7. The spectral features are roughly the same according to the 2D Fourier transform spectra (a)-(h) in Fig. 7 and 6. Actually, the dynamics along the waiting time T in Fig. 7(i) are same with that in Fig. 6(i). And the oscillation frequency of the signal reflected in Fig. 7(j) are also similar. It indicates that the shared modes only affect the amplitude of the signal without causing additional decoherence.

VI. CONCLUSIONS AND REMARKS

In this paper, we have theoretically derived the nonlinear responses of 2PPE and 3PPE using a nonperturbative approach, starting from the Hamiltonian with and without environment, and obtained the analytical expressions of the response functions based on a three-level V-type system.

In 2PPE, our methods are same with the traditional methods, with only a slight difference in amplitude. In 3PPE, the expressions have additional fifth- and seventh-order terms compared to that in the perturbation method. In order to explore the effect of these higher-order terms. We then utilize the Kubo model and find that in the case of strong coupling, the nonperturbative approach shows additional features in the signal. During the dynamics at time T , the oscillatory behaviors of the diagonal and off-diagonal peaks has changed greatly, and these changes come from the contributions of higher-order terms. However, in the case of weak coupling, the changes of the oscillatory behaviors are not obvious. Our nonperturbative approach is more suitable than the perturbative method for strong coupling.

Finally, we further examine the impact of the shared mode. We found that the shared mode only affects the amplitude of the signal without causing additional decoherence in the dynamics along time T .

-
- [1] S. Mukamel, *Principles of Nonlinear Optical Spectroscopy* (1995).
 - [2] M. Cho, *Two-Dimensional Optical Spectroscopy* (CRC Press, 2009).
 - [3] P. Hamm and M. Zanni, *Concepts and Methods of 2D Infrared Spectroscopy* (Cambridge University Press, 2009).
 - [4] W. Domcke and G. Stock, in *Adv. Chem. Phys.* (John Wiley &

- Sons, Inc., 1997) pp. 1–169.
- [5] J. Sung and R. J. Silbey, *J. Chem. Phys.* **115**, 9266 (2001).
- [6] J. Sung and R. J. Silbey, *J. Chem. Phys.* **118**, 2443 (2003).
- [7] K. Wuthrich, *NMR of proteins and nucleic acids* (John Wiley and Sons: New York, 1986).
- [8] R. R. Ernst, G. Bodenhausen, and A. Wokaun, *Principles of Nuclear Magnetic Resonance in One and Two Dimensions* (Ox-

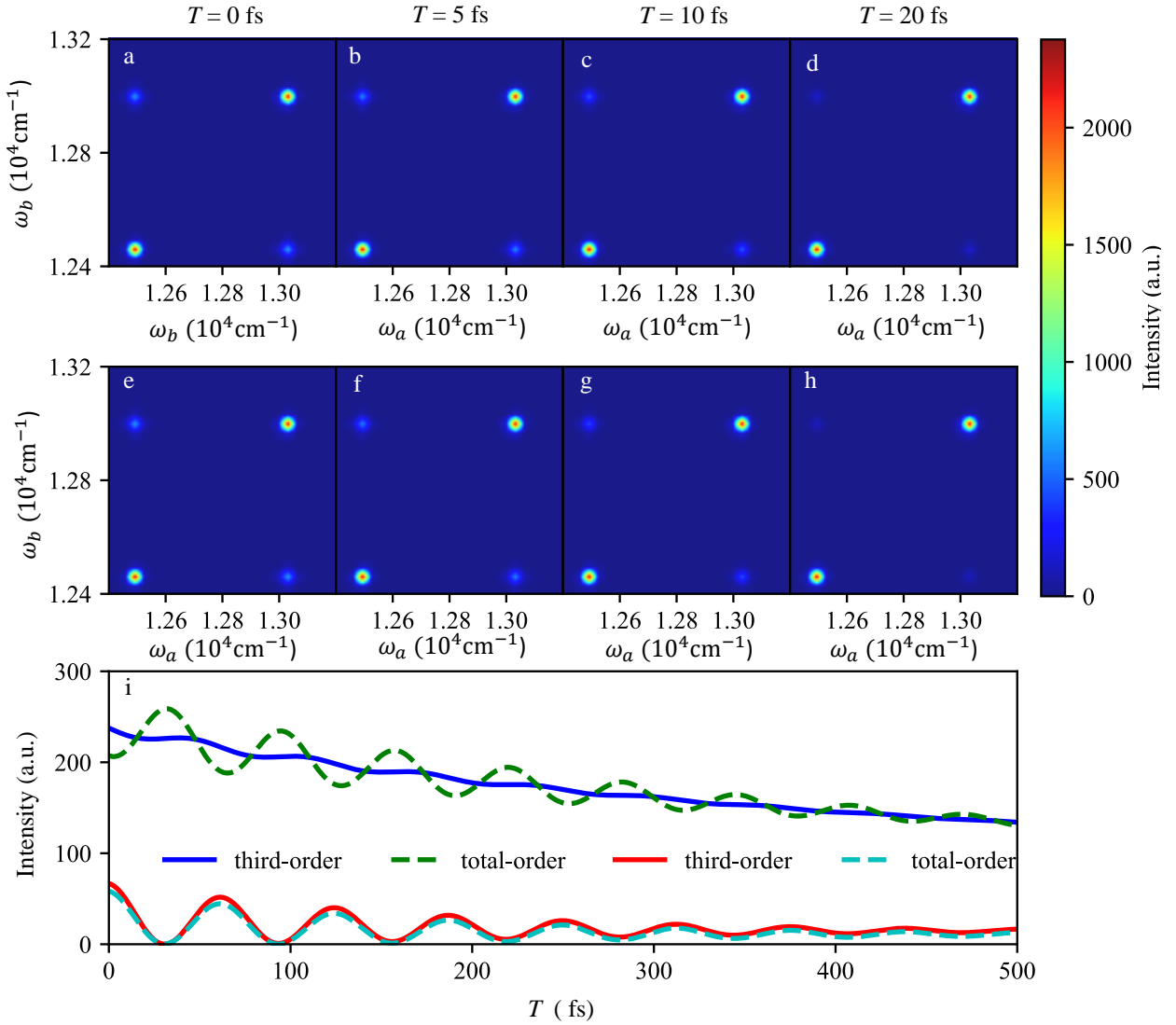


Figure 5. (Color online) 2D spectra and the dynamics along the waiting time T for the weak interaction. (a)-(d) the third-order terms and (e)-(f) the total-order terms for $T = 0, 5, 10, 20$ fs, respectively. (i) the dynamics along the waiting time T for the diagonal (ω_a, ω_a) and off-diagonal (ω_a, ω_b) peaks for third-order terms and total-order terms. The solid blue and dashed green lines describe the information of the diagonal peak, and the solid red line and dashed cyan lines describe the information of the off-diagonal peak. These spectra for any fixed T are obtained via 2D fast Fourier transform of the time domain signal scanned from 0 to 5 ps with 0.5 fs time step for both τ and t . In the figure, we plot the absolute values of the transform result. And the coupling strengths between system and electric field are $\Omega_a = 53\text{cm}^{-1}$ and $\Omega_b = 53\text{cm}^{-1}$.

ford University Press, 1987).

- [9] Y. J. Yan and S. Mukamel, *J. Chem. Phys.* **94**, 179 (1991).
- [10] G. R. Fleming and M. Cho, *Annu. Rev. Phys. Chem.* **47**, 109 (1996).
- [11] T. Joo, Y. Jia, J.-Y. Yu, M. J. Lang, and G. R. Fleming, *J. Chem. Phys.* **104**, 6089 (1996).
- [12] D. M. Jonas, *Annu. Rev. Phys. Chem.* **54**, 425 (2003).
- [13] T. Brixner, J. Stenger, H. M. Vaswani, M. Cho, R. E. Blankenship, and G. R. Fleming, *Nature* **434**, 625 (2005).
- [14] A. D. Hammerich, R. Kosloff, and M. A. Ratner, *J. Chem. Phys.* **97**, 6410 (1992).
- [15] U. Banin, A. Bartana, S. Ruhman, and R. Kosloff, *J. Chem. Phys.* **101**, 8461 (1994).
- [16] G. Ashkenazi, U. Banin, A. Bartana, R. Kosloff, and S. Ruhman, in *Adv. Chem. Phys.* (John Wiley & Sons, Inc., 2007) pp. 229–315.
- [17] L. Xu, H. Dong, and L. Fu, *Opt. Lett.* **43**, 5725 (2018).
- [18] L. Seidner, G. Stock, and W. Domcke, *J. Chem. Phys.* **103**, 3998 (1995).
- [19] B. Wolfseder, L. Seidner, G. Stock, and W. Domcke, *Chem.*

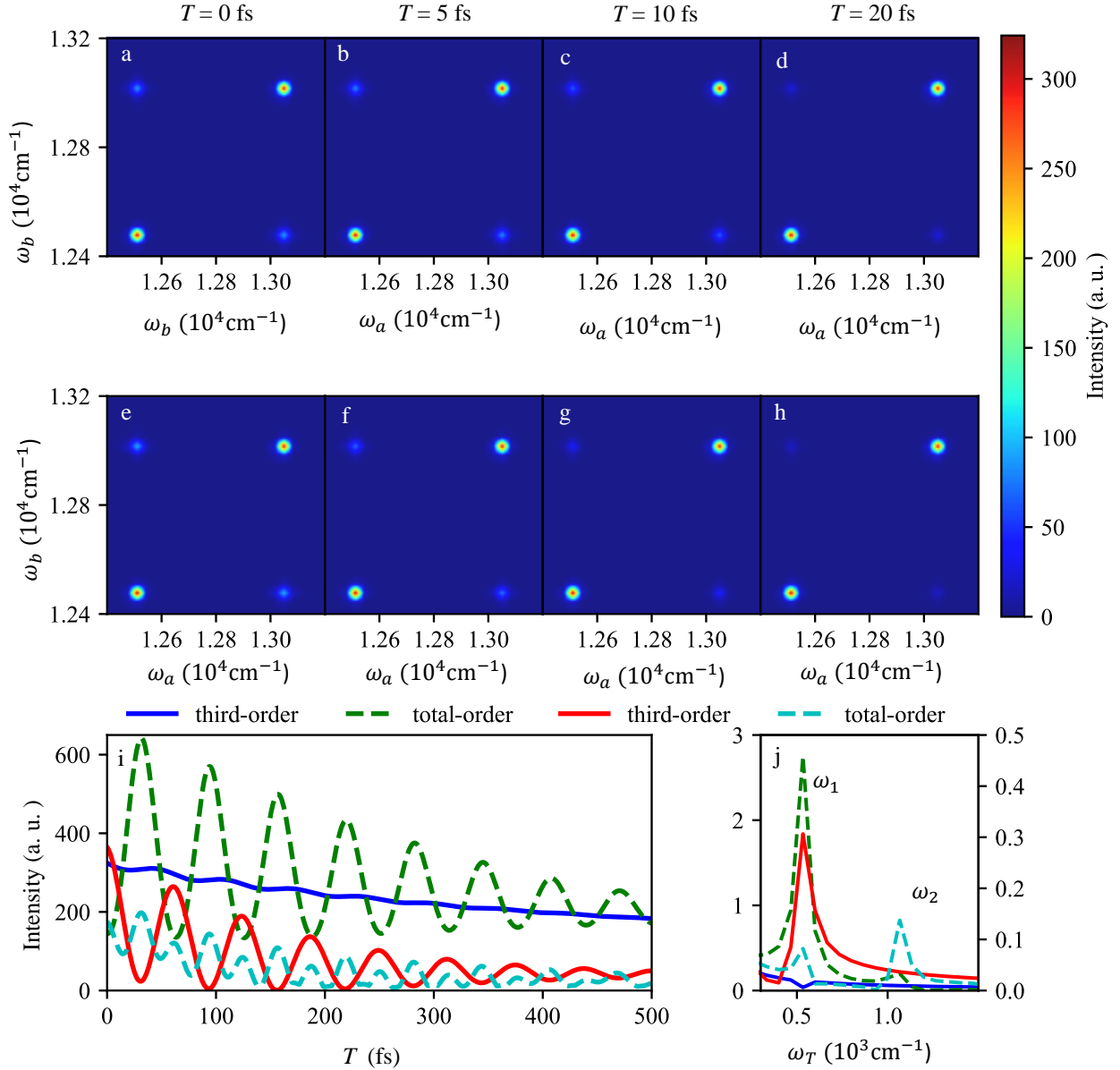


Figure 6. (Color online) 2D spectra and the dynamics along the waiting time T for the strong interaction. (a)-(d) the third-order terms and (e)-(h) the total-order terms for $T = 0, 5, 10, 20$ fs, respectively. The coupling strengths between system and electric field are $\Omega_a = 106\text{cm}^{-1}$ and $\Omega_b = 106\text{cm}^{-1}$. (i) the dynamics along the waiting time T for the diagonal (ω_a, ω_a) and off-diagonal (ω_a, ω_b) peaks for third-order terms and total-order terms. (j) the Fast Fourier Transform shows the frequency of oscillation of each line in (i).

- Phys. **217**, 275 (1997).
- [20] M. F. Gelin, A. V. Pisiakov, D. Egorova, and W. Domcke, *J. Chem. Phys.* **118**, 5287 (2003).
- [21] M. F. Gelin, D. Egorova, and W. Domcke, *J. Chem. Phys.* **123**, 164112 (2005).
- [22] J. Faeder, I. Pinkas, G. Knopp, Y. Prior, and D. J. Tannor, *J. Chem. Phys.* **115**, 8440 (2001).
- [23] C. P. Koch, T. KlÄEner, and R. Kosloff, *J. Chem. Phys.* **116**, 7983 (2002).
- [24] D. Gelman, G. Katz, R. Kosloff, and M. A. Ratner, *J. Chem. Phys.* **123**, 134112 (2005).
- [25] T. I. C. Jansen, J. G. Snijders, and K. Duppen, *J. Chem. Phys.* **113**, 307 (2000).
- [26] T. I. C. Jansen, J. G. Snijders, and K. Duppen, *J. Chem. Phys.* **114**, 10910 (2001).
- [27] T. Mančal, A. V. Pisiakov, and G. R. Fleming, *J. Chem. Phys.*

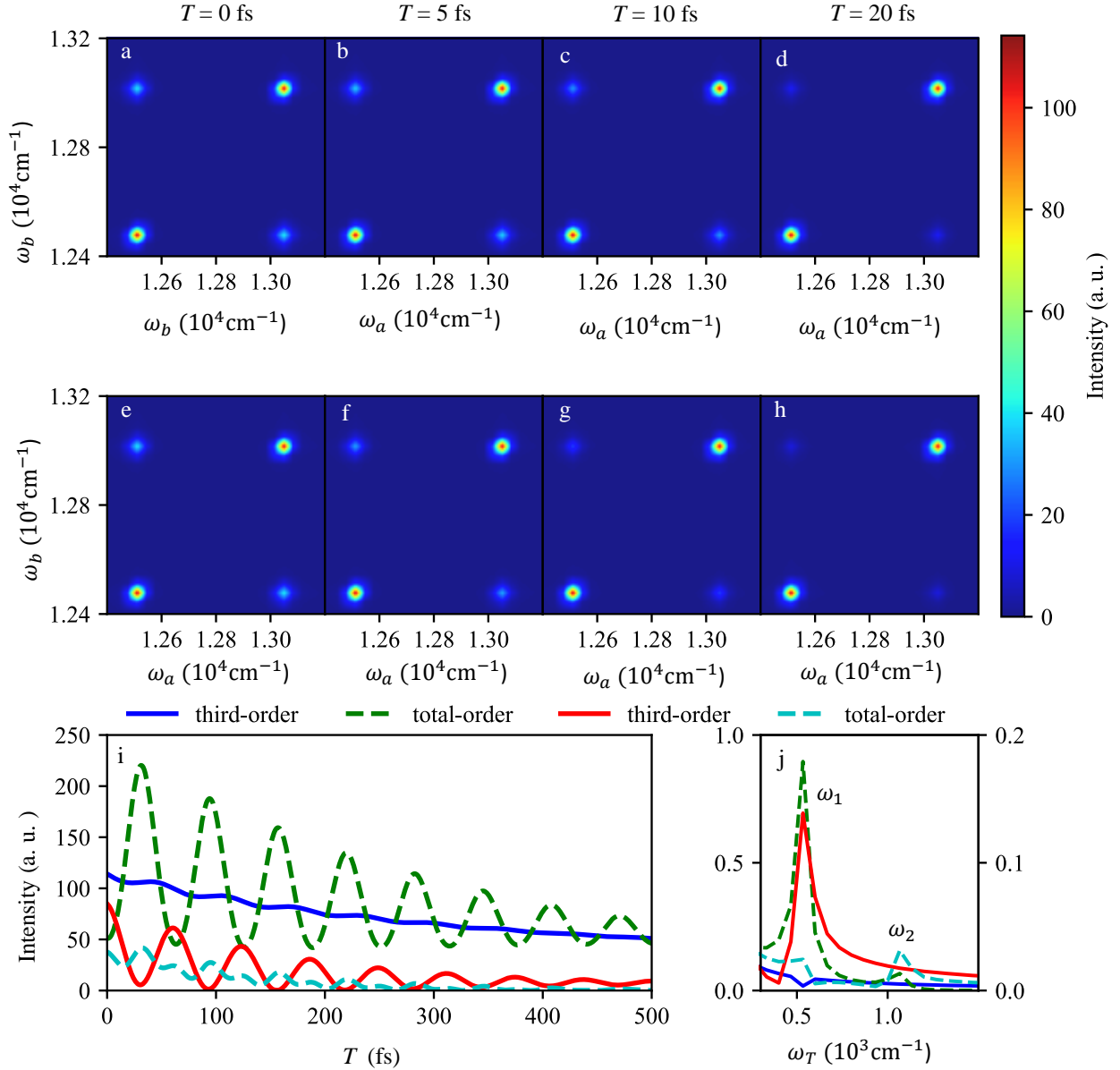


Figure 7. (Color online) 2D spectra and the dynamics along the waiting time T for the strong interaction containing shared modes c_j . The parameters are the same as in Fig. 6.

- 124, 234504 (2006).
- [28] A. V. Pislakov, T. Mančal, and G. R. Fleming, *J. Chem. Phys.* **124**, 234505 (2006).
- [29] B. J. Ka and E. Geva, *J. Chem. Phys.* **125**, 214501 (2006).
- [30] B. BrÄeggemann, P. Kjellberg, and T. Pullerits, *Chem. Phys. Lett.* **444**, 192 (2007).
- [31] V. V. Strelkov, *Phys. Rev. A* **93**, 053812 (2016).
- [32] O. Reshef, E. Giese, M. Z. Alam, I. D. Leon, J. Upham, and R. W. Boyd, *Opt. Lett.* **42**, 3225 (2017).
- [33] A. Guandalini, C. Cocchi, S. Pittalis, A. Ruini, and C. A. Rozzi, *Phys. Chem. Chem. Phys. PCCP* **23**, 10059 (2021).
- [34] M. O. Scully and M. S. Zubairy, *Quantum Optics* (1999).
- [35] J.-P. Likforman, M. Joffre, and V. Thierry-Mieg, *Opt. Lett.* **22**, 1104 (1997).
- [36] W. P. de Boeij, M. S. Pshenichnikov, and D. A. Wiersma, *Annu. Rev. Phys. Chem.* **49**, 99 (1998).
- [37] X. J. Jordanides, M. J. Lang, X. Song, and G. R. Fleming, *J. Phys. Chem. B* **103**, 7995 (1999).
- [38] R. Agarwal, B. S. Prall, A. H. Rizvi, M. Yang, and G. R. Fleming, *J. Chem. Phys.* **116**, 6243 (2002).

- [39] M. Scully, M. J. Stephen, and D. C. Burnham, *Phys. Rev.* **171**, 213 (1968).
 [40] S. Jang, Y.-C. Cheng, D. R. Reichman, and J. D. Eaves, *J. Chem. Phys.* **129**, 101104 (2008).
 [41] S. Jang, *J. Chem. Phys.* **131**, 164101 (2009).
 [42] E. Hennebicq, D. Beljonne, C. Curutchet, G. D. Scholes, and R. J. Silbey, *J. Chem. Phys.* **130**, 214505 (2009).
 [43] H. Dong and G. R. Fleming, *J. Phys. Chem. B* **118**, 8956 (2014).
 [44] A. Tokmakoff, (2011).
 [45] R. Kubo, *A stochastic theory of line shape* (1969).
 [46] E. Hanamura, *J. Phys. Soc. Japan* **52**, 2258 (1983).

Appendix A: Evolution of three-level system under laser pulse

The three levels are denoted as g , a and b . The Hamiltonian of the three-level V-type system is $H_0 = \hbar\omega_g |g\rangle \langle g| + \hbar\omega_a |a\rangle \langle a| + \hbar\omega_b |b\rangle \langle b|$, with $\omega_b \approx \omega_a > \omega_g$. To simplify the formula, we set $\omega_g = 0$. Interacting with the laser pulse, the system is coupled to the laser field

$$H_I = - [\hbar\Omega_a e^{-i\nu_a t + i\mathbf{k}\cdot\mathbf{r}} |a\rangle \langle g| + \text{h.c.}] - [\hbar\Omega_b e^{-i\nu_b t + i\mathbf{k}\cdot\mathbf{r}} |b\rangle \langle g| + \text{h.c.}], \quad (\text{A1})$$

where ν is the frequency of laser field with the wavevector \mathbf{k} . And in the interaction picture, the Hamiltonian would be time-independent,

$$H_I^{\text{int}} = - [\hbar\Omega_a e^{i\mathbf{k}\cdot\mathbf{r}} |a\rangle \langle g| + \text{h.c.}] - [\hbar\Omega_b e^{i\mathbf{k}\cdot\mathbf{r}} |b\rangle \langle g| + \text{h.c.}]. \quad (\text{A2})$$

The general solution of the current system under the interaction with laser pulse can be presented by the state as

$$|\Psi(t)\rangle = C_g(t) |g\rangle + C_a(t) |a\rangle + C_b(t) |b\rangle,$$

where

$$\begin{aligned} C_g(t) &= C_g(0) \cos \Omega t + i \left(\frac{\Omega_a e^{-i\mathbf{k}\cdot\mathbf{r}}}{\Omega} C_a(0) + \frac{\Omega_b e^{-i\mathbf{k}\cdot\mathbf{r}}}{\Omega} C_b(0) \right) \sin \Omega t, \\ C_a(t) &= i \frac{\Omega_a e^{i\mathbf{k}\cdot\mathbf{r}}}{\Omega} \sin \Omega t C_g(0) + \frac{\Omega_b^2 + \Omega_a^2 \cos \Omega t}{\Omega^2} C_a(0) + \frac{[\cos \Omega t - 1] \Omega_a \Omega_b}{\Omega^2} C_b(0), \\ C_b(t) &= i \frac{\Omega_b e^{i\mathbf{k}\cdot\mathbf{r}}}{\Omega} \sin \Omega t C_g(0) + \frac{[\cos \Omega t - 1] \Omega_a \Omega_b}{\Omega^2} C_a(0) + \frac{\Omega_a^2 + \Omega_b^2 \cos \Omega t}{\Omega^2} C_b(0). \end{aligned} \quad (\text{A3})$$

For the special cases that is initially on the ground state $C_g(0) = 1$ to be used in the derivation, we have

$$C_g(t) = \cos \Omega t, \quad (\text{A4})$$

$$C_a(t) = i \frac{\Omega_a e^{i\mathbf{k}\cdot\mathbf{r}}}{\Omega} \sin \Omega t, \quad (\text{A5})$$

$$C_b(t) = i \frac{\Omega_b e^{i\mathbf{k}\cdot\mathbf{r}}}{\Omega} \sin \Omega t. \quad (\text{A6})$$

Appendix B: The state after evolution

We first give the exact expression of the state in 2PPE. The state of the system without environment after the two pulses with a delay τ can be written as

$$\begin{aligned}
& |\psi_2(T, \tau)\rangle \\
&= \left[\cos \theta_1 \cos \theta_2 - e^{i(\mathbf{k}_1 - \mathbf{k}_2) \cdot \mathbf{r}} \sin \theta_1 \sin \theta_2 \left(\frac{\Omega_a^2}{\Omega^2} e^{-i\omega_a \tau} + \frac{\Omega_b^2}{\Omega^2} e^{-i\omega_b \tau} \right) \right] |g\rangle \\
&\quad + i \cos \theta_1 \sin \theta_2 \frac{\Omega_a e^{i\mathbf{k}_2 \cdot \mathbf{r} - i\omega_a T}}{\Omega} |a\rangle \\
&\quad + i \frac{\sin \theta_1 e^{i\mathbf{k}_1 \cdot \mathbf{r} - i\omega_a T}}{\Omega^3} \left(\Omega_a (\Omega_b^2 + \Omega_a^2 \cos \theta_2) e^{-i\omega_a \tau} + [\cos \theta_2 - 1] \Omega_a^2 \Omega_b e^{-i\omega_b \tau} \right) |a\rangle \\
&\quad + i \cos \theta_1 \sin \theta_2 \frac{\Omega_b e^{i\mathbf{k}_2 \cdot \mathbf{r} - i\omega_b T}}{\Omega} |b\rangle \\
&\quad + i \frac{\sin \theta_1 e^{i\mathbf{k}_1 \cdot \mathbf{r} - i\omega_b T}}{\Omega^3} \left([\cos \theta_2 - 1] \Omega_a^2 \Omega_b e^{-i\omega_a \tau} + \Omega_b (\Omega_a^2 + \Omega_b^2 \cos \theta_2) e^{-i\omega_b \tau} \right) |b\rangle. \tag{B1}
\end{aligned}$$

The state of the system coupled with environment after the two pulses with a delay τ can be written as

$$\begin{aligned}
& |\psi_2(\tau, T)\rangle \\
&= \left[c_1 c_2 e^{-iH_g(T+\tau)} - \eta_a^2 s_1 s_2 e^{i(\mathbf{k}_1 - \mathbf{k}_2) \cdot \mathbf{r} - i\omega_a \tau} e^{-iH_g T} e^{-iH_a \tau} - \eta_b^2 s_1 s_2 e^{i(\mathbf{k}_1 - \mathbf{k}_2) \cdot \mathbf{r} - i\omega_b \tau} e^{-iH_g T} e^{-iH_b \tau} \right] |g\alpha\beta\chi\rangle \tag{B2} \\
&\quad + \left[i\eta_a c_1 s_2 e^{i\mathbf{k}_2 \cdot \mathbf{r} - i\omega_a T} e^{-iH_a T} e^{-iH_g \tau} + i\eta_a s_1 (\eta_b^2 + \eta_a^2 c_2) e^{i\mathbf{k}_1 \cdot \mathbf{r} - i\omega_a \tau - i\omega_a T} e^{-iH_a T} e^{-iH_a \tau} \right. \\
&\quad \quad \left. + i\eta_b s_1 (c_2 - 1) \eta_a \eta_b e^{i\mathbf{k}_1 \cdot \mathbf{r} - i\omega_b \tau - i\omega_a T} e^{-iH_a T} e^{-iH_b \tau} \right] |a\alpha\beta\chi\rangle \\
&\quad + \left[i\eta_b c_1 s_2 e^{i\mathbf{k}_2 \cdot \mathbf{r} - i\omega_b T} e^{-iH_b T} e^{-iH_g \tau} + i\eta_a s_1 (c_2 - 1) \eta_a \eta_b e^{i\mathbf{k}_1 \cdot \mathbf{r} - i\omega_a \tau - i\omega_b T} e^{-iH_b T} e^{-iH_a \tau} \right. \\
&\quad \quad \left. + i\eta_b s_1 (\eta_a^2 + \eta_b^2 c_2) e^{i\mathbf{k}_1 \cdot \mathbf{r} - i\omega_b \tau - i\omega_b T} e^{-iH_b T} e^{-iH_b \tau} \right] |b\alpha\beta\chi\rangle. \tag{B3}
\end{aligned}$$

We then give the exact expression of the state in 3PPE. The state of the system coupled with environment after the three pulses with a delay τ and T can be written as

$$\begin{aligned}
& |\psi_3(\tau, T, t)\rangle \\
&= \left[c_1 |g\rangle e^{-iH_g t} + i\eta_a s_3 |a\rangle e^{i\mathbf{k}_3 \cdot \mathbf{r} - i\omega_a t - iH_a t} + i\eta_b s_3 |b\rangle e^{i\mathbf{k}_3 \cdot \mathbf{r} - i\omega_b t - iH_b t} \right] \\
&\quad \otimes \left[c_1 c_2 e^{-iH_g(T+\tau)} - \eta_a^2 s_1 s_2 e^{i(\mathbf{k}_1 - \mathbf{k}_2) \cdot \mathbf{r} - i\omega_a \tau} e^{-iH_g T} e^{-iH_a \tau} \right. \\
&\quad \quad \left. - \eta_b^2 s_1 s_2 e^{i(\mathbf{k}_1 - \mathbf{k}_2) \cdot \mathbf{r} - i\omega_b \tau} e^{-iH_g T} e^{-iH_b \tau} \right] |\alpha\beta\chi\rangle \\
&\quad + \left[i\eta_a s_3 |g\rangle e^{-i\mathbf{k}_3 \cdot \mathbf{r} - iH_g t} + (\eta_b^2 + \eta_a^2 c_3) |a\rangle e^{-i\omega_a t - iH_a t} + (c_3 - 1) \eta_a \eta_b |b\rangle e^{-i\omega_b t - iH_b t} \right] \\
&\quad \otimes \left[i\eta_a c_1 s_2 e^{i\mathbf{k}_2 \cdot \mathbf{r} - i\omega_a T} e^{-iH_a T} e^{-iH_g \tau} + i\eta_a s_1 (\eta_b^2 + \eta_a^2 c_2) e^{i\mathbf{k}_1 \cdot \mathbf{r} - i\omega_a (\tau+T)} e^{-iH_a (\tau+T)} \right. \\
&\quad \quad \left. + i\eta_a \eta_b^2 s_1 (c_2 - 1) e^{i\mathbf{k}_1 \cdot \mathbf{r} - i\omega_b \tau - i\omega_a T} e^{-iH_a T} e^{-iH_b \tau} \right] |\alpha\beta\chi\rangle \\
&\quad + \left[i\eta_b s_3 |g\rangle e^{-i\mathbf{k}_3 \cdot \mathbf{r} - iH_g t} + (c_3 - 1) \eta_a \eta_b |a\rangle e^{-i\omega_a t - iH_a t} + (\eta_a^2 + \eta_b^2 c_3) |b\rangle e^{-i\omega_b t - iH_b t} \right] \\
&\quad \otimes \left[i\eta_b c_1 s_2 e^{i\mathbf{k}_2 \cdot \mathbf{r} - i\omega_b T} e^{-iH_b T} e^{-iH_g \tau} + i\eta_a s_1 (c_2 - 1) e^{i\mathbf{k}_1 \cdot \mathbf{r} - i\omega_a \tau - i\omega_b T} e^{-iH_b T} e^{-iH_a \tau} \right. \\
&\quad \quad \left. + i\eta_a \eta_b^2 s_1 (\eta_a^2 + \eta_b^2 c_2) e^{i\mathbf{k}_1 \cdot \mathbf{r} - i\omega_b (\tau+T)} e^{-iH_b (\tau+T)} \right] |\alpha\beta\chi\rangle. \tag{B4}
\end{aligned}$$

Appendix C: Trajectory dephasing factor

The trajectory factors $\mathcal{D}_{aa}(\tau, T; \alpha\beta\chi)$ and $\mathcal{D}_8(\tau, T, t; \alpha, \beta, \chi)$ in 2PPE and 3PPE, respectively, are presented. By computing the evolution of the coherent state and taking the overlap, we can get

$$\begin{aligned}
\mathcal{D}_{aa}(\tau, T; \alpha\beta\chi) &= \exp(-2g_a^{0*}(\tau) - g_a^{0*}(T) - g_a^0(T) + g_a^{0*}(\tau + T)) \\
&\quad \times \exp(-2\mathcal{C}_a^{0*}(\tau) - \mathcal{C}_a^{0*}(T) - \mathcal{C}_a^0(T) + \mathcal{C}_a^{0*}(\tau + T)) \\
&\quad \times \exp\{i2[w\text{Im}(\alpha)(1 - 2\cos\omega\tau + \cos(\omega(T + \tau))) + w\text{Re}(\alpha)(2\sin\omega\tau - \sin(\omega(T + \tau)))]\} \\
&\quad \times \exp\{i2[u_a\text{Im}(\chi)(1 - 2\cos\mu\tau + \cos(\mu(T + \tau))) + u_a\text{Re}(\chi)(2\sin\mu\tau - \sin(\mu(T + \tau)))]\}. \tag{C1}
\end{aligned}$$

$$\begin{aligned}
\mathcal{D}_8(\tau, T, t; \alpha, \beta, \chi) = & \exp[-g_a^{0*}(T + \tau) - g_b^0(t + T)] \\
& \times \exp[-\mathcal{C}_{bb}^0(t + T) - \mathcal{C}_{aa}^{0*}(T + \tau) - \mathcal{C}_{ab}^{0*}(\tau) + \mathcal{C}_{ab}^{0*}(T + t + \tau) + \mathcal{C}_{ab}^{0*}(T) - \mathcal{C}_{ab}^{0*}(t)] \\
& \exp(i2w[\text{Re}(\alpha)\sin(\omega(T + \tau)) + \text{Im}(\alpha)(1 - \cos(\omega(T + \tau)))]]) \\
& \exp(i2v[\text{Re}(\beta)(\sin(\nu\tau) - \sin(\nu(T + \tau + t))) + \text{Im}(\beta)(-\cos(\nu\tau) + \cos(\nu(T + \tau + t)))]]) \\
& \exp\{i2\text{Re}(\chi)(u_b\sin(\mu\tau) - u_b\sin(\mu(T + t + \tau)) + u_a\sin(\mu(T + \tau)))\} \\
& \exp\{i2\text{Im}(\chi)(-u_b\cos(\mu\tau) + u_a + u_b\cos(\mu(T + t + \tau))) - u_a\cos(\mu(T + \tau))\}. \tag{C2}
\end{aligned}$$

The other trajectory factors are also calculated in the same way.

Appendix D: Three-pulse photon echo dephasing factor

Through the simple multivariate Gaussian integration of trajectory factors the with respect to α , β and χ in 3PPE, the trajectory dephasing factors of each term are given. The trajectory dephasing factors of the third-order terms are

$$\begin{aligned}
D_1(\tau, T, t) = & \exp[-g_a^*(\tau) - g_a^*(T + \tau) + g_a^*(T + t + \tau) + g_a^*(T) - g_a^*(T + t) - g_a(t)] \\
& \times \exp[-\mathcal{C}_{aa}^*(\tau) - \mathcal{C}_{aa}^*(T + \tau) + \mathcal{C}_{aa}^*(T + t + \tau) + \mathcal{C}_{aa}^*(T) - \mathcal{C}_{aa}^*(T + t) - \mathcal{C}_{aa}(t)], \\
D_2(\tau, T, t) = & \exp[-g_b^*(\tau) - g_b^*(T + \tau) + g_b^*(T + t + \tau) + g_b^*(T) - g_b^*(T + t) - g_b(t)] \\
& \times \exp[-\mathcal{C}_{bb}^*(\tau) - \mathcal{C}_{bb}^*(T + \tau) + \mathcal{C}_{bb}^*(T + t + \tau) + \mathcal{C}_{bb}^*(T) - \mathcal{C}_{bb}^*(T + t) - \mathcal{C}_{bb}(t)], \\
D_3(\tau, T, t) = & \exp[-g_a(t) - g_b^*(\tau)] \\
& \times \exp[-\mathcal{C}_{aa}(t) - \mathcal{C}_{bb}^*(\tau) - \mathcal{C}_{ab}^*(T + \tau) + \mathcal{C}_{ab}^*(T + t + \tau) + \mathcal{C}_{ab}^*(T) - \mathcal{C}_{ab}^*(T + t)], \\
D_4(\tau, T, t) = & \exp[-g_a^*(\tau) - g_b(t)] \\
& \times \exp[-\mathcal{C}_{aa}^*(\tau) - \mathcal{C}_{bb}(t) - \mathcal{C}_{ab}^*(T + \tau) + \mathcal{C}_{ab}^*(T + t + \tau) + \mathcal{C}_{ab}^*(T) - \mathcal{C}_{ab}^*(T + t)], \\
D_5(\tau, T, t) = & \exp[-g_a^*(T + \tau) - g_a^*(\tau) + g_a^*(T + t + \tau) + g_a(T) - g_a^*(t) - g_a(T + t)] \\
& \times \exp[-\mathcal{C}_{aa}^*(T + \tau) - \mathcal{C}_{aa}^*(\tau) + \mathcal{C}_{aa}^*(T + t + \tau) + \mathcal{C}_{aa}(T) - \mathcal{C}_{aa}^*(t) - \mathcal{C}_{aa}(T + t)], \\
D_6(\tau, T, t) = & \exp[-g_b^*(T + \tau) - g_b^*(\tau) + g_b^*(T + t + \tau) + g_b(T) - g_b^*(t) - g_b(T + t)] \\
& \times \exp[-\mathcal{C}_{bb}^*(T + \tau) - \mathcal{C}_{bb}^*(\tau) + \mathcal{C}_{bb}^*(T + t + \tau) + \mathcal{C}_{bb}(T) - \mathcal{C}_{bb}^*(t) - \mathcal{C}_{bb}(T + t)], \\
D_7(\tau, T, t) = & \exp[-g_a(T + t) - g_b^*(T + \tau)] \\
& \times \exp[-\mathcal{C}_{aa}(T + t) - \mathcal{C}_{bb}^*(\tau + T) - \mathcal{C}_{ab}^*(\tau) - \mathcal{C}_{ab}^*(t) + \mathcal{C}_{ab}(T) + \mathcal{C}_{ab}^*(\tau + T + t)], \\
D_8(\tau, T, t) = & \exp[-g_a^*(T + \tau) - g_b(t + T)] \\
& \times \exp[-\mathcal{C}_{bb}(t + T) - \mathcal{C}_{aa}^*(T + \tau) - \mathcal{C}_{ab}^*(\tau) + \mathcal{C}_{ab}^*(T + t + \tau) + \mathcal{C}_{ab}(T) - \mathcal{C}_{ab}^*(t)]. \tag{D1}
\end{aligned}$$

The trajectory dephasing factors of the fifth-order terms are

$$\begin{aligned}
D_9(\tau, T, t) &= \exp(-g_a^*(t) + g_a^*(T+t) - g_a(T+t) - g_a^*(T) + g_a(T) - g_b^*(\tau)) \\
&\quad \times \exp(-\mathcal{C}_{aa}^*(t) + \mathcal{C}_{aa}^*(T+t) - \mathcal{C}_{aa}(T+t) - \mathcal{C}_{aa}^*(T) + \mathcal{C}_{aa}(T) - \mathcal{C}_{bb}^*(\tau)) \\
&\quad \times \exp(\mathcal{C}_{ab}^*(T+t+\tau) - \mathcal{C}_{ab}^*(T+t) - \mathcal{C}_{ab}^*(T+\tau) + \mathcal{C}_{ab}^*(T)), \\
D_{10}(\tau, T, t) &= \exp(-g_a^*(\tau) - g_b^*(t) + g_b^*(T+t) - g_b(T+t) - g_b^*(T) + g_b(T)) \\
&\quad \times \exp(-\mathcal{C}_{aa}^*(\tau) - \mathcal{C}_{bb}^*(t) + \mathcal{C}_{bb}^*(T+t) - \mathcal{C}_{bb}(T+t) - \mathcal{C}_{bb}^*(T) + \mathcal{C}_{bb}(T)) \\
&\quad \times \exp(\mathcal{C}_{ab}^*(T+t+\tau) - \mathcal{C}_{ab}^*(T+t) - \mathcal{C}_{ab}^*(T+\tau) + \mathcal{C}_{ab}^*(T)), \\
D_{11}(\tau, T, t) &= \exp(-g_a^*(\tau) - g_b(t) - \mathcal{C}_{aa}^*(\tau) - \mathcal{C}_{bb}(t)) \\
&\quad \times \exp(-\mathcal{C}_{ab}^*(T+\tau) + \mathcal{C}_{ab}^*(T+\tau+T) + \mathcal{C}_{ab}(T) - \mathcal{C}_{ab}(T+t) + \mathcal{C}_{ab}(t) - \mathcal{C}_{ab}^*(t)), \\
D_{12}(\tau, T, t) &= \exp(-g_a(t) - g_b^*(\tau) - \mathcal{C}_{aa}(t) - \mathcal{C}_{bb}^*(\tau)) \\
&\quad \times \exp(-\mathcal{C}_{ab}^*(T+\tau) + \mathcal{C}_{ab}^*(T+\tau+t) + \mathcal{C}_{ab}(T) - \mathcal{C}_{ab}(T+t) + \mathcal{C}_{ab}(t) - \mathcal{C}_{ab}^*(t)), \\
D_{13}(\tau, T, t) &= \exp(-2g_a^*(\tau) + g_a^*(T+t+\tau) - g_a(T+t) - g_a^*(T+t) - g_b^*(T)) \\
&\quad \times \exp(-2\mathcal{C}_{aa}^*(\tau) + \mathcal{C}_{aa}^*(T+t+\tau) - \mathcal{C}_{aa}(T+t) - \mathcal{C}_{aa}^*(T+t) - \mathcal{C}_{bb}^*(T)) \\
&\quad \times \exp(\mathcal{C}_{ab}^*(\tau) - \mathcal{C}_{ab}^*(T+\tau) + \mathcal{C}_{ab}^*(T+t) - \mathcal{C}_{ab}^*(t) + \mathcal{C}_{ab}(T) + \mathcal{C}_{ab}^*(T)), \\
D_{14}(\tau, T, t) &= \exp(-g_a^*(T) - 2g_b^*(\tau) + g_b^*(T+t+\tau) - g_b(T+t) - g_b^*(T+t)) \\
&\quad \times \exp(-\mathcal{C}_{aa}^*(T) - 2\mathcal{C}_{bb}^*(\tau) + \mathcal{C}_{bb}^*(T+t+\tau) - \mathcal{C}_{bb}(T+t) - \mathcal{C}_{bb}^*(T+t)) \\
&\quad \times \exp(\mathcal{C}_{ab}^*(\tau) - \mathcal{C}_{ab}^*(T+\tau) + \mathcal{C}_{ab}^*(T+t) - \mathcal{C}_{ab}^*(t) + \mathcal{C}_{ab}(T) + \mathcal{C}_{ab}^*(T)) \\
D_{15}(\tau, T, t) &= \exp(-g_a(T) - g_b(t) - g_b^*(t) + g_b^*(T+\tau+t) - 2g_b^*(T+\tau)) \\
&\quad \times \exp(-\mathcal{C}_{aa}(T) - \mathcal{C}_{bb}(t) - \mathcal{C}_{bb}^*(t) + \mathcal{C}_{bb}^*(T+\tau+t) - 2\mathcal{C}_{bb}^*(T+\tau)) \\
&\quad \times \exp(\mathcal{C}_{ab}^*(T+\tau) - \mathcal{C}_{ab}^*(\tau) + 2\mathcal{C}_{ab}(T) + \mathcal{C}_{ab}(t) - \mathcal{C}_{ab}(T+t)) \\
D_{16}(\tau, T, t) &= \exp(-g_b(T) - g_a(t) - g_a^*(t) + g_a^*(T+\tau+t) - 2g_a^*(T+\tau)) \\
&\quad \times \exp(-\mathcal{C}_{bb}(T) - \mathcal{C}_{aa}(t) - \mathcal{C}_{aa}^*(t) + \mathcal{C}_{aa}^*(T+\tau+t) - 2\mathcal{C}_{aa}^*(T+\tau)) \\
&\quad \times \exp(\mathcal{C}_{ab}^*(T+\tau) - \mathcal{C}_{ab}^*(\tau) + 2\mathcal{C}_{ab}(T) + \mathcal{C}_{ab}(t) - \mathcal{C}_{ab}(T+t)). \tag{D2}
\end{aligned}$$

The trajectory dephasing factors of the seventh-order terms are

$$\begin{aligned}
D_{17}(\tau, T, t) &= \exp(-g_a^*(\tau) - g_a^*(T+\tau) + g_a^*(T+\tau+t) + g_a^*(T) - g_a^*(T+t) - g_a(t)) \\
&\quad \times \exp(-\mathcal{C}_{aa}^*(\tau) - \mathcal{C}_{aa}^*(T+\tau) + \mathcal{C}_{aa}^*(T+\tau+t) + \mathcal{C}_{aa}^*(T) - \mathcal{C}_{aa}^*(T+t) - \mathcal{C}_{aa}(t)), \\
D_{18}(\tau, T, t) &= \exp(-g_b^*(\tau) - g_b^*(T+\tau) + g_b^*(T+\tau+t) + g_b^*(T) - g_b^*(T+t) - g_b(t)) \\
&\quad \times \exp(-\mathcal{C}_{bb}^*(\tau) - \mathcal{C}_{bb}^*(T+\tau) + \mathcal{C}_{bb}^*(T+\tau+t) + \mathcal{C}_{bb}^*(T) - \mathcal{C}_{bb}^*(T+t) - \mathcal{C}_{bb}(t)), \\
D_{19}(\tau, T, t) &= \exp(-2g_a^*(\tau) - g_a^*(T) - g_a(T) + g_a^*(T+\tau) - 2g_b^*(T) - g_b^*(t) - g_b(t) + g_b^*(T+t)) \\
&\quad \times \exp(-2\mathcal{C}_{aa}^*(\tau) - \mathcal{C}_{aa}^*(T) - \mathcal{C}_{aa}(T) + \mathcal{C}_{aa}^*(T+\tau) - 2\mathcal{C}_{bb}^*(T) - \mathcal{C}_{bb}^*(t) - \mathcal{C}_{bb}(t) + \mathcal{C}_{bb}^*(T+t)) \\
&\quad \times \exp(\mathcal{C}_{ab}^*(\tau) - 2\mathcal{C}_{ab}^*(T+\tau) + \mathcal{C}_{ab}^*(T+\tau+t) + 3\mathcal{C}_{ab}^*(T) + 2\mathcal{C}_{ab}(T) - \mathcal{C}_{ab}(T+t) - \mathcal{C}_{ab}^*(T+t) + \mathcal{C}_{ab}(t)), \\
D_{20}(\tau, T, t) &= \exp(-2g_b^*(\tau) - g_b^*(T) - g_b(T) + g_b^*(T+\tau) - 2g_a^*(T) - g_a^*(t) - g_a(t) + g_a^*(T+t)) \\
&\quad \times \exp(-2\mathcal{C}_{bb}^*(\tau) - \mathcal{C}_{bb}^*(T) - \mathcal{C}_{bb}(T) + \mathcal{C}_{bb}^*(T+\tau) - 2\mathcal{C}_{aa}^*(T) - \mathcal{C}_{aa}^*(t) - \mathcal{C}_{aa}(t) + \mathcal{C}_{aa}^*(T+t)) \\
&\quad \times \exp(\mathcal{C}_{ab}^*(\tau) - 2\mathcal{C}_{ab}^*(T+\tau) + \mathcal{C}_{ab}^*(T+\tau+t) + 3\mathcal{C}_{ab}^*(T) + 2\mathcal{C}_{ab}(T) - \mathcal{C}_{ab}(T+t) - \mathcal{C}_{ab}^*(T+t) + \mathcal{C}_{ab}(t)). \tag{D3}
\end{aligned}$$